

Dark gas in the Solar neighborhood from extinction data

D. Paradis^{1,2}, K. Dobashi³, T. Shimoikura³, A. Kawamura⁴, T. Onishi⁵, Y. Fukui⁴, and J.-P. Bernard^{1,2}

¹ Université de Toulouse; UPS-OMP; IRAP; Toulouse, France

² CNRS; IRAP; 9 Av. du Colonel Roche, BP 44346, Toulouse, cedex 4, France

³ Department of Astronomy and Earth Sciences, Tokyo Gakugei University, Koganei, Tokyo 184-8501, Japan

⁴ Department of Astrophysics, Nagoya University, Chikusa-ku, Nagoya 464-8602, Japan

⁵ Department of Physical Science, Osaka Prefecture University, Gakuen 1-1, Sakai, Osaka 599-8531, Japan

Preprint online version: January 8, 2019

ABSTRACT

Context. When modeling infrared or γ -ray data as a linear combination of observed gas tracers, an excess of emission has been pointed out with respect to expectations from known neutral and atomic gas as traced by HI and CO measurements respectively. This excess could result from an additional gas component. This gas, called "dark-gas" (DG) has been observed in our Galaxy, as well as in the Magellanic Clouds.

Aims. In this paper, we investigate for the first time the correlation between visible extinction (A_V) data and the gas tracers on large scales in the solar neighborhood, to evidence the presence of DG, and to check the compatibility with previous studies.

Methods. Our work focuses on the solar neighborhood ($|b| > 10^\circ$), as well as the inner and outer Galaxy and on four individual regions: Taurus, Orion, Cepheus-Polaris and Aquila-Ophiuchus. Thanks to the recent production of an all-sky A_V map, we first perform the correlation between A_V and HI and CO emission over the most diffuse regions (with low-intermediate gas column densities), to derive the optimal $(A_V/N_H)^{\text{ref}}$ ratio. We then iterate the analysis over the entire regions (including low and high gas column densities) to estimate the CO-to- H_2 conversion factor as well as the DG mass fraction.

Results. The average extinction to gas column density ratio in the solar neighborhood is found to be $(A_V/N_H)^{\text{ref}} = 6.53 \times 10^{-22}$ mag. cm^2 , with significant differences between the inner and outer Galaxy, of about 60%. We derive an average value of the CO-to- H_2 conversion factor of $X_{\text{CO}} = 1.67 \times 10^{20} \text{ H}_2 \text{ cm}^{-2}/(\text{K km s}^{-1})$, with significant variations between nearby clouds. In the solar neighborhood, the gas mass in the dark component is found to be 19% relative to that in the atomic component and 164% relative to the one traced by CO. These results are compatible with the recent analysis using Planck data within the uncertainties of our measurements. We estimate the fraction of dark gas to the total molecular gas to be 0.62 in the solar neighborhood. The HI-to- H_2 and H_2 -to-CO transitions appear for $A_V \approx 0.2$ and $A_V \approx 1.5$, respectively, in agreement with theoretical models of dark- H_2 gas.

Key words. ISM:dust, extinction - ISM: clouds - solar neighborhood

1. Introduction

The interstellar medium (ISM) is composed of gas and dust, with a mass contribution of the dust component of about 1% of the total ISM mass. Interstellar gas provides the material for star-formation, making it a central part in the life cycle of matter. The gas is either atomic, molecular, or ionized and these three phases are commonly observed using the HI 21 cm emission, CO transitions and H_α or free-free emission respectively. Several studies have reported an emission excess in the far-infrared (FIR) with respect to the gas, correlated with none of the gas tracers. These evidences have first been obtained for Galactic regions (Reach et al., 1994; Meyerdierks & Heithausen, 1996). By analyzing the diffuse γ -ray emission from the ISM, Grenier et al. (2005) concluded to the presence of an additional gas phase in our Galaxy, called "dark gas" (DG), with a non-negligible mass. This component has also been pointed out in the Magellanic clouds (Leroy et al., 2007; Bernard et al., 2008; Roman-Duval et al., 2010).

Recently, Planck collaboration (2011a) obtained all-sky maps of the dust optical depth and, comparing it with the observed gas column density, constructed a map of the DG distribution covering a large fraction of the intermediate latitude sky ($|b| > 10^\circ$). On average, they estimated the mass of DG to

be 28% of the atomic mass and to be 118% of the molecular gas traced by CO emission in the solar neighborhood. The results indicate that the DG appears for intermediate hydrogen column densities, corresponding to extinctions values between 0.4 and 2.5 mag. The first possible explanation is that the DG could be molecular gas, not detected using the CO(J=1-0) transition. Indeed, it is expected that a layer of pure H_2 , or with dissociated CO should exist around dense clouds (e.g. Wolfire et al., 2010) that would not be detectable, because at temperatures below 100 K (typical of such environments), the fluxes from the H_2 rotational transitions are too low. However, it can also be traced using other species such as C^+ (see Langer et al., 2010). Other possible origins have been pointed in Planck collaboration (2011a) to explain the observed departure from linearity between the dust optical depth (τ) and the observable gas column density: (1)-variations in the dust/gas ratio (D/G), (2)-weak CO emission not detected at the sensitivity of the CO survey, (3)-optically thin approximation for the HI emission not valid over the entire sky, (4)-formation of dust aggregates, inducing a higher dust emissivity. Concerning hypothesis (1), the authors concluded that variations in D/G of about 30% are unlikely in the solar neighborhood. Assumptions (2) and (3) have been tested by carrying the analysis with an upper limit in the weak CO emission in one case, and with a different HI spin temperature in the other case. The authors deduced that

these two effects could not account for the whole excess. The last option (4) can be tested using extinction data, since dust aggregates are expected to have an increased FIR emissivity, but mostly unaffected optical properties in the visible and ultra-violet. Therefore no substantial A_V excess compared to gas column density should be observed in that case. It is to be noted that γ -ray observations would not detect any excess if the FIR excess was due to D/G or dust optical property variations.

The large dust particles that emit in the far-infrared (FIR) are also responsible for the main extinction in the visible and near-infrared (NIR). Extinction data are therefore well suited to check for the presence of DG. A recent extinction map covering the whole sky has been produced using the 2 Micron All Sky Survey Point Source Catalog (2MASS PSC) by Dobashi (2011). This map has since significantly been improved to correct for the background star intrinsic colors (Dobashi et al., 2012).

This study is carried out following the methodology adopted in Planck collaboration (2011a), but using extinction instead of FIR optical depth. Using dust optical depth requires to determine dust temperature and therefore making assumptions about the dust emissivity shape and/or mixing effects along the line-of-sight (LOS). On the other hand, in principle, extinction measures dust column density directly. In practice however, large scale extinction maps derived from star counts have limited accuracy and suffer from bias inherent to the fact that stars are intermixed with the gas, and star light does not sample the whole LOS. In this analysis we use the same gas tracers as in Planck collaboration (2011a), so that the results can be compared directly

Here, we want to compare the spatial distribution of the DG seen in absorption and emission, as well as the DG masses derived from the two approaches. We also want to investigate, whether the transition between the HI and H₂ phases is consistent with that found using FIR emission. In addition, we are interested in comparing our results with theoretical models such as that of Wolfire et al. (2010).

In Section 2 we present the dataset used in this analysis, then in Section 3.1 we describe the method we applied to perform the correlations between extinction data and gas tracers. We discuss the results in Section 4. Finally, a summary of our findings is provided in Section 5.

2. Observations

2.1. Extinction data

We used color excess maps produced by Dobashi (2011) based on the 2MASS PSC (Skrutskie et al., 2006). The maps are derived using a technique named “the X percentile method” (Dobashi et al., 2008, 2009) which is a new extension of the well-known NICE method introduced by Lada et al. (1994). While the standard NICE method uses the mean color of stars found in a cell set on the sky to measure the color excess by dust, the X percentile method utilizes the X percentile reddest star ($X = 100\%$ is the reddest) and it is characterized by being robust against contamination by the unreddened foreground stars.

The combination of the maps (Galactic plane, north and south high latitudes sky) cover the whole sky with a $1'$ grid and a varying angular resolution (from $1'$ to $12'$) because of the “the adaptive grid” mapping technique used (Cambr esy, 1999). This technique adjusts the resolution to include a constant number of stars in the cells to measure the color excess in order to keep a flat noise level all over the sky.

Among the color excess maps presented by Dobashi (2011), we selected the E(J–H) map measured in the range $50 < X < 95\%$ (based on his equation 4) to compare with the gas data, because the map is relatively more sensitive compared to other maps and has less defects in the regions studied in this paper ($|b| > 10^\circ$). However, note that the results obtained in the following do not change significantly when using other maps computed at different X values or from the other color excess available, E(H–K_S).

Here, we should note that there is a slight but systematic offsets in the original color excess maps of Dobashi (2011) arising from the rather ambiguous determination of the background star colors, i.e., the mean star colors unreddened by dust, which is needed to determine the zero point of the color excess. In general, when deriving a color excess map on large scale using the NICE method, it is virtually impossible to determine the background star colors precisely from the observed stars themselves, because the mean intrinsic star colors should vary on the sky and there is no region without dust along the galactic plane. For simplicity, Dobashi (2011) assumed a constant mean intrinsic star color in all directions, like for other all-sky color excess maps derived in a similar way, e.g., by Rowles and Froebrich (2009). This leads to a systematic offset in the final color excess map.

This varying offset is generally not large, but can cause significant problems when attempting to detect DG. In order to reduce such offsets, we use the new color excess maps by Dobashi et al. (2012) who gave a correction to the original color excess maps of Dobashi (2011), by determining the mean intrinsic star colors as a function of Galactic coordinates, using the Besan on Galactic model (Robin et al., 2003) which is one of the latest Galactic stellar population synthesis model. Based on this model, they generated a star catalog equivalent to the 2MASS PSC, but free from any interstellar dust, and calculated how the mean intrinsic star colors vary across the sky when applying the X percentile method to the simulated star catalog. They regarded the resulting star color maps as the background for the color excess maps derived from the 2MASS PSC.

In addition, Dobashi et al. (2012) further estimated what fraction of the total dust along the LOS escapes detection by the X percentile method, by simulating the effect of a diffuse dust disk on the simulated star catalog. The method is known to underestimate the diffuse dust component extending over a large region along the LOS, while it can retrieve extinction from individual well-defined dark clouds more precisely (Dobashi et al., 2009). As a result, they found that more than 80 % of the total dust along the LOS should be detected in the Galactic latitude range $|b| \gtrsim 5^\circ$, though the effect is more severe in the lower latitude range (e.g., by $\sim 50\%$ at $|b| \approx 0^\circ$). They derived a map of the detection rate of the dust disk, which can be used to correct the color excess maps for the underestimation at large scales.

The color excess maps used in this work were corrected for the background star colors as well as for the underestimation of the diffuse extended dust component. However, the corrected maps might still be erroneous close to $|b| \approx 0^\circ$, especially around the Galactic center, because of the inhomogeneous detection limits in the 2MASS PSC and/or unknown stellar populations not taken into account in the Besan on Model. Therefore, when we compare the maps with the gas data in the following, we restrict ourselves to $|b| > 10^\circ$, where these corrections for the background and the underestimation are minimized. This also corresponds to the region studied in Planck collaboration (2011a).

Finally, we converted the E(J–H) map to A_V using:

$$A_V = 10.9E(J - H) \quad (1)$$

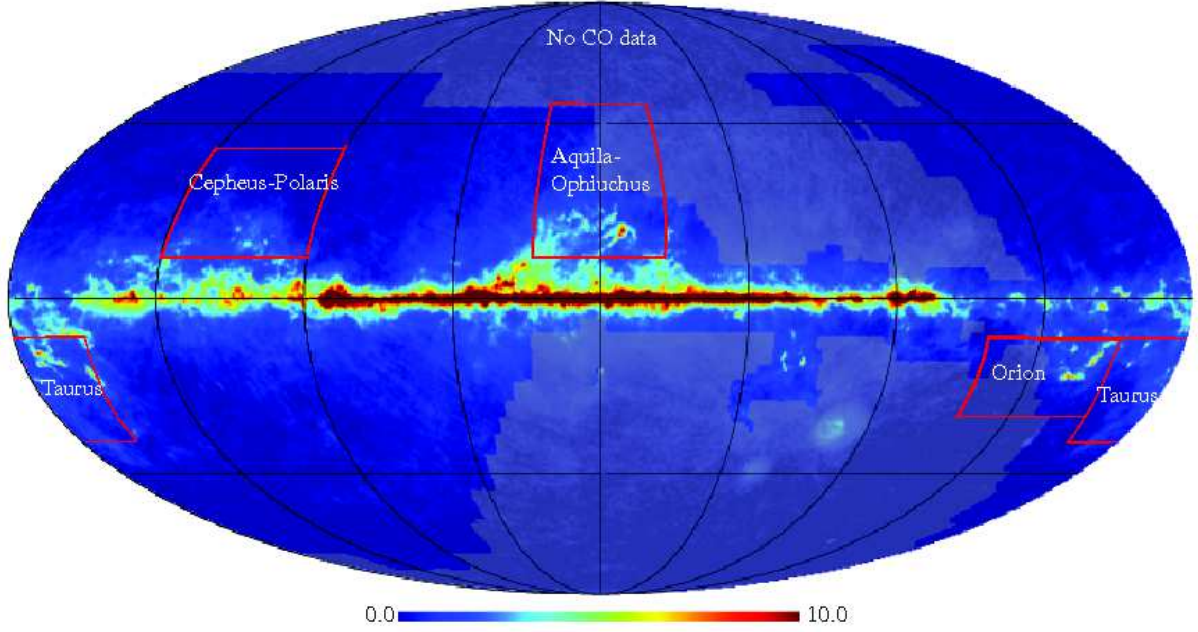


Fig. 1. Extinction map (A_V) in mag. Regions in light blue are not covered by the combination of the Dame et al. (2001) and NANTEN CO surveys, and are not used in our analyses. The red boxes correspond to individual regions defined in Section 3.1.3.

where the coefficient corresponds to the empirical reddening law by Cardelli et al. (1989) for $R_V = 3.1$. The resulting map (see Figure 1) has an almost constant noise level of $\Delta A_V \approx 0.5$ mag.

2.2. Gas tracers

The gas tracers used in this analysis are the same as described in Planck collaboration (2011a). Here we provide a summary of the atomic (21 cm HI emission) and molecular ($^{12}\text{CO}(J=1-0)$ line) surveys. We use the LAB (Leiden/Argentine/Bonn) survey to trace the atomic gas. This survey is the combination of the Leiden/Dwingeloo survey by Hartmann & Burton (1997), with sky observations above -30° of Galactic latitude (at a $36'$ angular resolution), and the IAR (Instituto Argentino de Radioastronomía) survey (Arnal et al., 2000; Bajaja et al., 2005) of the Southern sky at latitudes below -25° (at a $30'$ angular resolution). The LAB data had been integrated in the velocity range $-400 < V_{\text{LSR}} < 400$ km s^{-1} . Assuming that the gas is optically thin, we deduce the hydrogen column density from the integrated intensity of the HI emission (W_{HI}) using:

$$N_{\text{HI}} = X_{\text{HI}} W_{\text{HI}} \quad (2)$$

with X_{HI} the HI integrated intensity to column density conversion factor. This factor is taken to be equal to 1.82×10^{18} H/cm 2 /(K km s^{-1}) (Spitzer, 1978).

For the molecular gas, we use the combination of three $^{12}\text{CO}(J=1-0)$ line surveys:

- The Dame et al. (2001) survey, in the Galactic plane, obtained with both CfA telescope in the north (at an angular resolution of $8.4'$) and CfA-Chile telescope in the south (at an angular resolution of $8.8'$). The integrated intensity map had been derived by integrating the velocity range where the CO emission is significantly detected (Dame, 2011);
- The unpublished high latitude survey obtained with the CfA telescope, still observing the northern sky (Dame et al.,

2012). The data cube had been integrated over 10-20 velocity channels;

- the NANTEN survey obtained from Chile for the intermediate Galactic latitudes not covered by the Dame et al. (2001) survey, at a $2.6'$ angular resolution. This survey is still unpublished, but a full description of the NANTEN telescope can be found in Fukui et al. (1999), for instance. The total intensity map had been obtained by integrating the data cube over the whole velocity range.

Each survey has been smoothed to a common resolution of $8.8'$ using the convolution by a Gaussian kernel. As quoted in Planck collaboration (2011a) the NANTEN data appear to be 24% higher than the values obtained with the CfA telescopes. This discrepancy is still not understood and following Planck collaboration (2011a), the NANTEN data have been decreased by 24%, before merging, therefore assuming the absolute scale of Dame et al. (2001). The total map used in this analysis is shown in Planck collaboration (2011a), Figure 1. The CO integrated intensity (W_{CO}) to column density conversion factor is derived from the relation:

$$N_{\text{H}_2} = X_{\text{CO}} W_{\text{CO}}. \quad (3)$$

The value of the CO conversion factor (X_{CO}) is still debated. This factor is also expected to vary over the sky. For this reason we do not make any assumption and X_{CO} will be derived from the correlations (see Section 3.1).

The contribution from the ionized hydrogen is neglected in this study. This assumption is reasonable since we do not consider the Galactic plane emission, which includes most of the ionized medium emission caused by the presence of HII regions. However, its possible low contribution at high latitudes, not correlated with atomic nor molecular-traced gas can be accounted for in the constant term (A_V^0) when performing the correlations (see Equation 4).

Region	$\left(\frac{A_V}{N_H}\right)^{ref}$	A_V^0	X_{CO}	M_H^X/M_H^{HI}	M_H^X/M_H^{CO}	f_{DG}	
	(10^{-22} mag. cm 2)	(10^{-2} mag)	(10^{20} H $_2$ cm $^{-2}$ /(K km s $^{-1}$))			This work	From previous works
All $ b > 10^\circ$	6.53±0.03	6.16±0.67	1.67±0.08	0.19±0.25	1.64±2.20	0.62	0.55 ^a
Inner Galaxy	8.72±0.04	5.81±0.16	2.28±0.11	0.24±0.38	2.43±3.84	0.71	–
Outer Galaxy	5.46±0.03	4.68±0.75	1.67±0.10	0.11±0.28	0.74±1.92	0.43	–
Cepheus-Polaris	6.01±0.14	7.93±1.33	1.37±0.34	0.04±0.71	0.17±3.02	0.15	0.1 ^b - 0.3 ^c
Taurus	5.33±0.21	0.91±0.01	2.27±0.90	0.42±0.02	0.76±0.03	0.43	0.3 ^b
Orion	3.41±0.11	7.47±0.29	2.84±0.92	0.45±0.12	0.66±0.18	0.40	0.1 ^b
Aquila-Ophiuchus	6.99±0.18	11.78±0.53	3.46±0.91	0.59±0.06	1.65±0.18	0.62	0.6 ^b

Table 1. Derived parameters and their 1- σ uncertainties, computed over different regions, for $|b| > 10^\circ$.

^a From Planck collaboration (2011a)

^b From Grenier et al. (2005)

^c From Abdo, et al. (2010)

This work is done at the resolution of the HI data, i. e. 36'. All data are projected using the HEALPix pixelization scheme (Hierarchical Equal Area isoLatitude Pixelization)¹ with nside=256, corresponding to a pixel size of 13.7'. The description of the projection method used is given in appendix A.

3. Extinction/gas correlation

3.1. $(A_V/N_H)^{ref}$ and X_{CO} determination

In Planck collaboration (2011a), the reference value of the ratio between the dust optical depth and the gas column densities ($\left(\frac{\tau}{N_H}\right)^{ref}$) has been determined from the correlation between τ and the gas tracers at low gas column density. We follow the same type of analysis and model the extinction (A_V^{mod}) in the portion of the sky covered by the infrared, atomic and CO-traced surveys, and for $|b| > 10^\circ$, as:

$$A_V^{mod} = \left(\frac{A_V}{N_H}\right)^{ref} (N_H^{HI} + 2X_{CO}W_{CO}) + A_V^0 \quad (4)$$

where $\left(\frac{A_V}{N_H}\right)^{ref}$ is the reference value of the ratio between visible extinction and gas column density, and A_V^0 is a constant, that can account for ionized gas and/or offset in the extinction map.

However, the A_V map is particularly noisy at low column density, which makes the estimate of $\left(\frac{A_V}{N_H}\right)^{ref}$ difficult. Therefore we adopt a slightly different approach compared to that in Planck collaboration (2011a). Our analysis is done in two steps: first we select regions with a limited amount of DG by identifying regions in Figure 8 of Planck collaboration (2011a) with DG column density N_H^X such that $N_H^X/N_H < 0.05$ and we also impose a low CO content ($W_{CO} < 0.2$ K km s $^{-1}$). For this region, which we refer to as “no DG”, we derive the best-fit parameters: $\left(\frac{A_V}{N_H}\right)^{ref}$ and A_V^0 using Eq. 4, but do not attempt to derive X_{CO} in this first step since the considered regions have little CO emission. Second, we repeat the same analysis including all pixels of the considered region included in the gas surveys (we refer to this region as “All”), while imposing the $\left(\frac{A_V}{N_H}\right)^{ref}$ and A_V^0 values derived in the first step and determine the best fit value for X_{CO} . We also compute the mass of DG from the difference between the best correlation and the data at that stage. The procedure above was applied both to the whole high latitude sky (see Sec. 3.1.1) and for a set of individual regions (see Sec. 3.1.3) and in all cases is restricted to $|b| > 10^\circ$.

¹ <http://lambda.gsfc.nasa.gov/>

Results of the correlations are presented in Table 1. The best-fit parameters are obtained from χ^2 minimization. Parameter uncertainties are derived from the difference between the minimum and maximum values of the parameters contained in interval $\Delta\chi^2$ corresponding to a confidence level of 68%. Note that, for the purpose of illustrating the A_V -gas correlations (see Fig. 2 and 3), we also carried the correlation in a region with $N_H^X/N_H > 0.05$, which we refer to as “DG” region.

3.1.1. High latitude regions ($|b| > 10^\circ$)

The correlation is first performed over the whole high latitude sky ($|b| > 10^\circ$) characterizing the solar neighborhood. Results are displayed in Figure 2 (top panels). Note that the linear fits (slope= $\left(\frac{A_V}{N_H}\right)^{ref}$) shown in the figures (red lines) have been constrained on the whole data in the “no DG” region, and not on the binned version shown by yellow dots. The corresponding lines are curved as plotted in log-log scale, because of the constant term. The investigation of this “no DG” region leads to an $(A_V/N_H)^{ref}$ ratio of 6.53×10^{-22} mag.cm 2 . This value is close to the reference value of 5.34×10^{-22} obtained by Bohlin et al. (1978) relevant to the solar neighborhood and the Galactic plane. The optimal X_{CO} is found close to 1.67×10^{20} H $_2$ cm $^{-2}$ /(K km s $^{-1}$). This value is lower than the findings of Planck collaboration (2011a), who derived an averaged $X_{CO}=2.54 \times 10^{20}$ H $_2$ cm $^{-2}$ /(K km s $^{-1}$), but in better agreement with the Galactic average of 1.9×10^{20} H $_2$ cm $^{-2}$ /(K km s $^{-1}$) (Strong & Mattox, 1996) and with the value of 1.8×10^{20} H $_2$ cm $^{-2}$ /(K km s $^{-1}$) derived by Dame et al. (2001) for $|b| > 5^\circ$.

Looking at Figure 2, one can discern a different behavior in the A_V versus N_H plots (with $N_H = N_H^{HI} + 2X_{CO}W_{CO}$), when comparing the “DG” and “no DG” regions at intermediate and high A_V . In the first case, looking at the binned data points the correlation shows an excess between $N_H \approx 4 \times 10^{20}$ cm $^{-2}$ ($A_V=0.2$ mag) and $N_H \approx 3 \times 10^{21}$ cm $^{-2}$ ($A_V=1.5$ mag) as compared to a linear fit, whereas we do not in the second case. Note that, due to the low signal-to-noise in the extinction data at low column densities, the location of these transitions are determined by eye here, while they resulted from a fit in Planck collaboration (2011a). These results reinforce the existence of an additional gas phase, with a spatial distribution found to be similar to that determined using the Planck data (Planck collaboration, 2011a). For comparison, these authors estimated the appearance of the excess at A_V ranging from 0.4 to 2.5 mag. However, results obtained by Planck collaboration (2011b), analyzing the diffuse ISM and Galactic halo, have revealed some residual emission in the infrared/HI correlation, between $N_H \approx 3 \times 10^{20}$ cm $^{-2}$ ($A_V \approx 0.15$

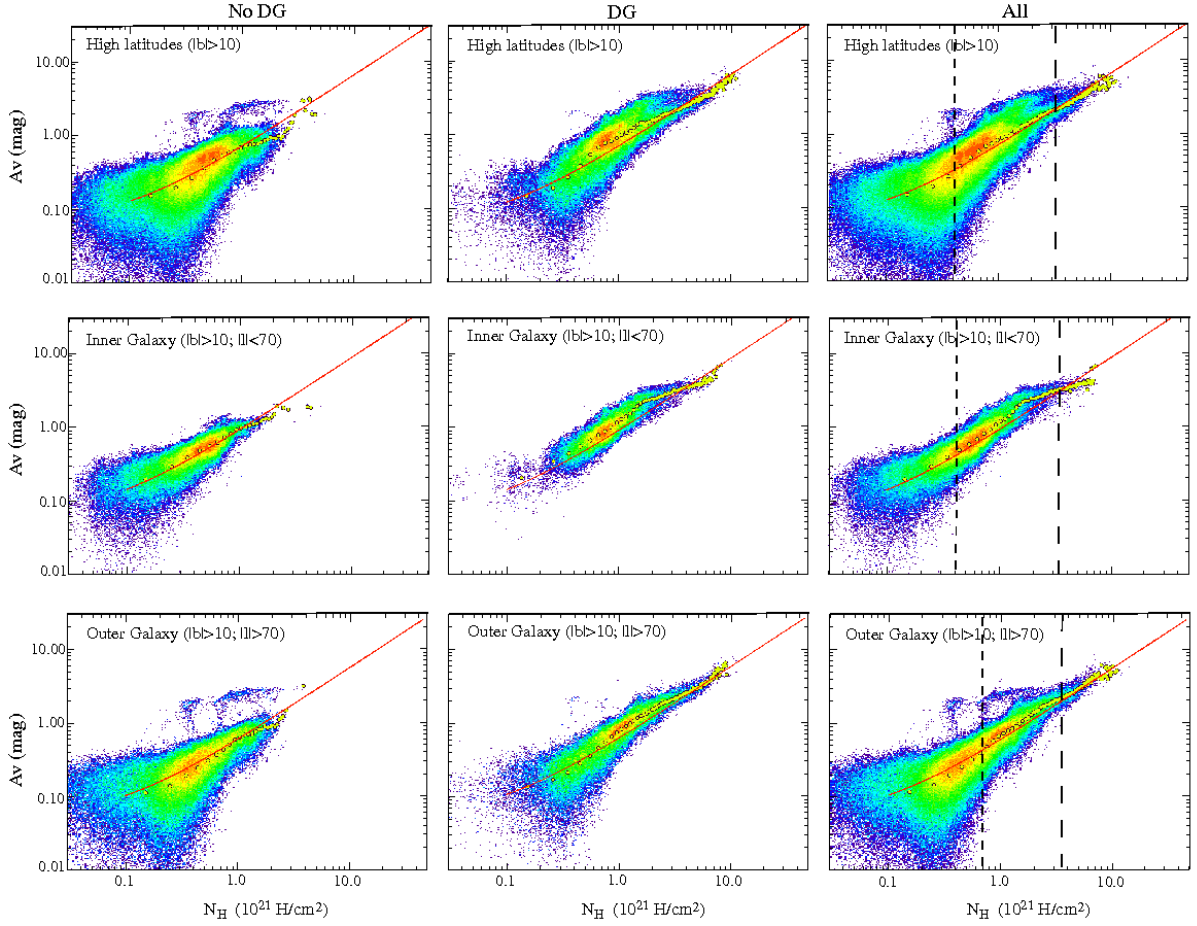


Fig. 2. Correlation plots between extinction data (A_V) and the total gas column density ($N_H = N_H^{\text{HI}} + 2X_{\text{CO}}W_{\text{CO}}$) excluding the Galactic plane ($|b| > 10^\circ$): high latitude sky (top panels), inner Galaxy (middle panels) and outer Galaxy (bottom panels). Left, middle and right panels correspond to respectively to regions where no DG is detected (“no DG”) according to Planck collaboration (2011a), where strong DG is detected (“DG”), and the entire region (“All”) (see Sec. 3.1). The color scale represents the density of pixels in log scale. The yellow dots show the correlation binned in N_H . The red lines show the best linear correlation, constrained on the whole data in the “no DG” region. The short-dashed and long-dashed lines indicate the position of a departure from a linear fit, and the position where the correlation recovers a linear behavior, respectively.

mag) and $N_H \simeq 4 \times 10^{21}$ ($A_V \simeq 2.0$ mag). Our results are intermediate between the two findings based on Planck data.

The column density of the dark component (N_H^X) can be computed as the difference between the observed and the best-fit (A_V^{mod}) extinction per unit column density, over the entire region:

$$N_H^X = \frac{A_V - A_V^{\text{mod}}}{(A_V/N_H)^{\text{ref}}}. \quad (5)$$

The total mass of hydrogen revealed by the DG component (M_H^X), the atomic (M_H^{HI}) and CO-traced molecular gas (M_H^{CO}), is estimated in the same way as in Planck collaboration (2011a):

$$M_H^{X, \text{HI}, \text{CO}} = m_H D^2 \Omega_{\text{pix}} \sum N_H^{X, \text{HI}, \text{CO}} \quad (6)$$

where D is the distance to the gas, m_H the hydrogen atom mass, and Ω_{pix} the pixel solid angle. As in Planck collaboration (2011a), we assume the same distance for all gas components. We obtain $M_H^X/M_H^{\text{HI}} = 0.19 \pm 0.25$ and $M_H^X/M_H^{\text{CO}} = 1.64 \pm 2.20$. These values are expected to be overestimate and underestimate, respectively, since the scale-height of the HI component is larger than that of the molecular one, with a probably intermediate scale-height for the DG component. The formal uncertainty on

the dark gas mass is large and essentially results from the assumed uncertainty on $\Delta A_V/A_V$ and from our assumption that this uncertainty is an absolute error and therefore does not scale down with the number of independent measurements. This leads to a large uncertainty on the DG mass when most pixels in a region have low A_V values, but it is likely that our assumption about the nature of the errors overestimates uncertainty.

Our DG mass is lower than found in Planck collaboration (2011a) who deduced $M_H^X/M_H^{\text{HI}} \simeq 0.28 \pm 0.03$ and $M_H^X/M_H^{\text{CO}} \simeq 1.18 \pm 0.01$, but consistent with it, taking our large uncertainties into account. With the use of their X_{CO} value we would obtain $M_H^X/M_H^{\text{CO}} \simeq 0.73$. Our results lead to a DG mass equal to 17% of the total observed mass, close to the value of 22% derived by Planck collaboration (2011a). Therefore, our study using extinction data reveals slightly less DG mass compared to the same analysis based on FIR data. The difference between the two analyses is however not significant due to large uncertainties for this region of the sky.

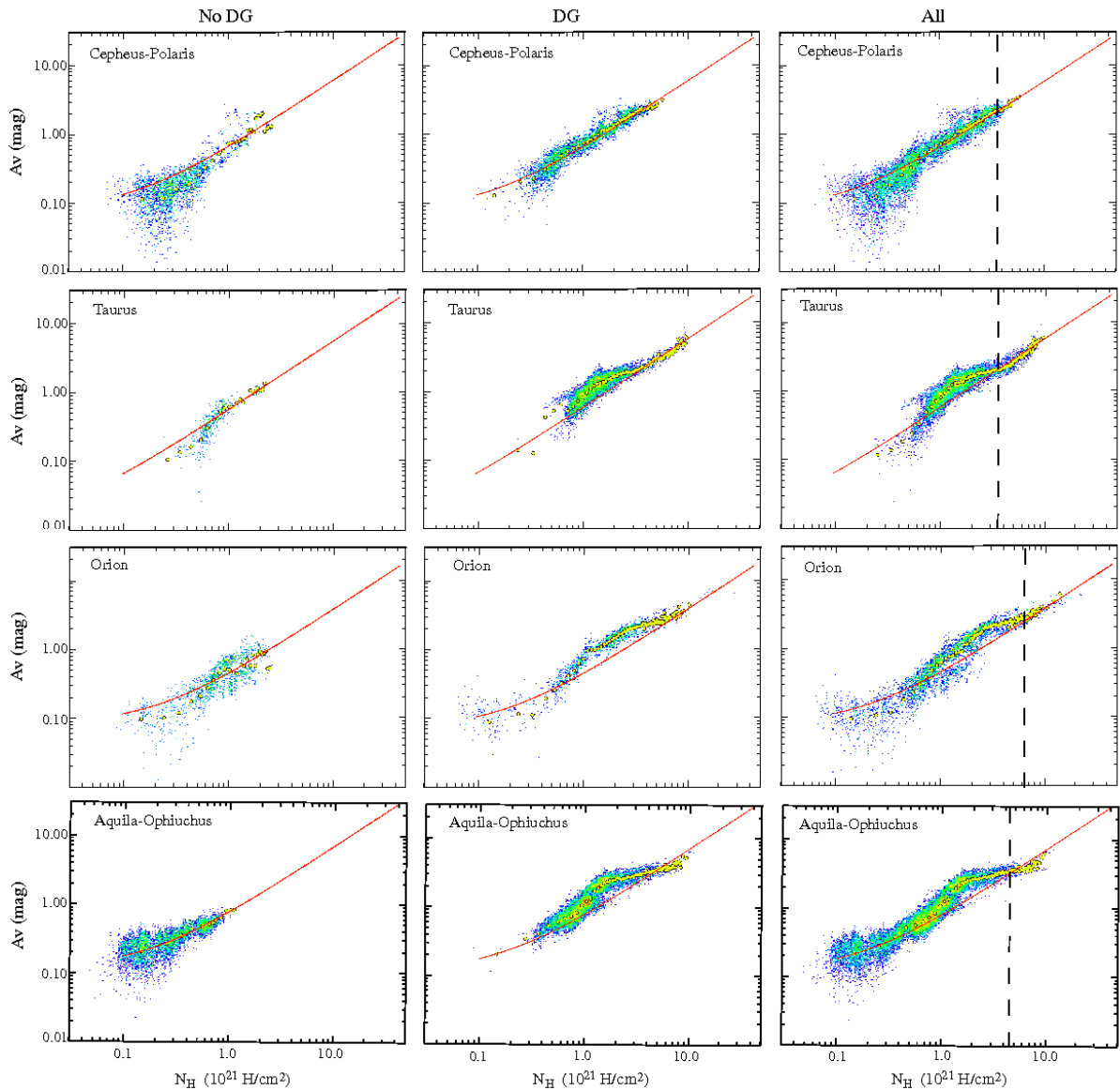


Fig. 3. Correlation plots between extinction data (A_V) and the total gas column density ($N_H = N_H^{\text{HI}} + 2X_{\text{CO}}W_{\text{CO}}$) in various regions excluding the Galactic plane ($|b| > 10^\circ$), from top to bottom: Cepheus-Polaris, Taurus, Orion, and Aquila-Ophiuchus region. Left, middle and right panels correspond to respectively to regions where no DG is detected (“no DG”) according to Planck collaboration (2011a), where strong DG is detected (“DG”), and the entire region (“All”) (see Sec. 3.1). The color scale represents the density of pixels in log scale. The description of the yellow dots, red and dashed lines is given in the caption of Figure 2.

3.1.2. Inner/outer Galaxy

We carry out the same analysis in the inner ($|l| < 70^\circ$) and outer ($|l| > 70^\circ$) Galaxy, at high latitudes ($|b| > 10^\circ$). A difference appears in the $(A_V/N_H)^{\text{ref}}$ ratio, with a higher value in the inner Galaxy ($((A_V/N_H)^{\text{ref}} = 8.72 \times 10^{-22} \text{ mag.cm}^{-2})$) compared to the outer Galaxy ($((A_V/N_H)^{\text{ref}} = 5.46 \times 10^{-22} \text{ mag.cm}^{-2})$). This result could illustrate true large scale variations in dust abundance and reflect the large scale metallicity gradient in our Galaxy.

From Figure 2, one can see that the excess is more prominent in the inner Galaxy than in the outer Galaxy. Also, we note that the outer Galaxy appears to be more noisy at low gas column densities. This is likely due to the fact that the outer Galaxy is hosting less stars than the inner Galaxy, inducing larger uncertainties in the resulting extinction map. The reconciliation be-

tween the data and the linear fit, corresponding to the H_2 -to-CO transition in the case of molecular DG, seems to occur at $N_H \approx 3 - 3.5 \times 10^{21}$ ($A_V \approx 1.5\text{-}1.75 \text{ mag}$) in both the inner and the outer Galaxy.

In term of the DG mass, each part of the Galaxy evidences distinct behaviors. Indeed, inner regions show an enhancement of the DG component, with ratios $M_{\text{H}}^{\text{X}}/M_{\text{H}}^{\text{HI}}$ and $M_{\text{H}}^{\text{X}}/M_{\text{H}}^{\text{CO}}$ of about 0.24 and 2.43, respectively. In contrast, the DG mass in the outer Galaxy represents only 11% of the gas in the atomic phase and 74% of that in the CO-traced phase. This result indicates that the additional gas phase is essentially concentrated in the inner Galaxy. In a similar way the X_{CO} factor appears to be larger in the inner Galaxy ($X_{\text{CO}} = 2.28 \times 10^{20} \text{ H}_2 \text{ cm}^{-2}/(\text{K km s}^{-1})$) than in the outer part ($X_{\text{CO}} = 1.67 \times 10^{20} \text{ H}_2 \text{ cm}^{-2}/(\text{K km s}^{-1})$).

3.1.3. Individual regions

Performing the analysis on individual regions requires the availability of enough pixels with and without DG, taking into account the limited extent of the CO survey. We were able to explore the A_V - N_H correlation in the following four regions:

- Taurus ($200^\circ < l < 160^\circ$; $-35^\circ < b < -10^\circ$)
- Orion ($240^\circ < l < 200^\circ$; $-30^\circ < b < -10^\circ$)
- Cepheus-Polaris ($135^\circ < l < 90^\circ$; $10^\circ < b < 40^\circ$)
- Aquila-Ophiuchus ($|l| < 20^\circ$; $10^\circ < b < 48^\circ$)

Results of the correlations for individual regions are presented in Figure 3. One can observe that regions located in the most external parts of the Galaxy, i. e. Taurus and Cepheus-Polaris, still suffer from A_V underestimate at low gas column densities. This is visible through pixels under the linear fit at low N_H . Each environment shows different dust properties, with $\left(\frac{A_V}{N_H}\right)^{\text{ref}}$ between 3.41×10^{-22} and 6.99×10^{-22} mag cm². Moreover, these regions are of high interest since they evidence distinct gas properties. The X_{CO} factor in Orion, and in Aquila-Ophiuchus are significantly larger than in the other regions. In addition, the former regions evidence a DG mass ratio relative to the atomic hydrogen substantially larger than in Taurus and Cepheus-Polaris, with ratios of 0.45 and 0.59 respectively. This large amount of DG in Orion and Aquila-Ophiuchus are visible in Figure 3 through the presence of a clear and important excess in the A_V - N_H plot. We have checked that the excess was not due to contamination by young stellar objects (YSOs). Indeed, the color excess maps may overestimate the true A_V if they are significantly contaminated by young stellar objects (YSOs). In these two regions we have therefore also performed the correlation between extinction maps in the J band (A_J) and the gas tracers, because YSOs would induce an underestimation in the extinction maps (as opposed to the color excess maps). The results indicate that the large amount of DG is not caused by the presence of YSOs. Grenier et al. (2005) obtained a ratio $M_{\text{H}^{\text{I}}}^{\text{X}}/M_{\text{H}^{\text{I}}}^{\text{HI}}$ even larger compared to our results, in the Aquila-Ophiuchus-Libra region, with a ratio of 1. In contrast, they derived a value of 0.14 in Orion. They found a ratio of 0.33 for the Taurus-Perseus-Triangulum region, close to our value of 0.42 in the Taurus region. We note however that the individual regions defined in Grenier et al. (2005) are not exactly the same as the ones used in this paper. The A_V - N_H plot for Cepheus-Polaris does not emphasize any noticeable excess. When comparing the DG mass with respect to the CO one in the different clouds, we observe significant variations. We note values going from 0.17 in the Cepheus-Polaris region to 1.65 in Aquila-Ophiuchus, with values of 0.66 and 0.76 in Orion and Taurus. These ratios are however highly dependent on the value of the X_{CO} factor. The low uncertainty of the dark mass in the Taurus region is caused by the relatively large A_V values. The absolute uncertainty $\Delta A_V/A_V$ is higher in Cepheus-Polaris that includes a large number of pixels at low A_V , inducing a considerable mass uncertainty.

The H₂-to-CO transition, which we determined by eye, appears at $N_H \approx 3.5 \times 10^{21}$ cm² ($A_V \approx 1.75$ mag) in Taurus, $N_H \approx 6 \times 10^{21}$ cm² ($A_V \approx 3.0$ mag) in Orion, $N_H \approx 3.5 \times 10^{21}$ cm² ($A_V \approx 1.75$ mag) in Cepheus-Polaris and at $N_H \approx 4 \times 10^{21}$ cm² ($A_V \approx 2.0$ mag) in Aquila-Ophiuchus. This transition seems to vary with environment. The position of the HI-to-H₂ transition is uncertain because of the noise in the extinction data at low gas column densities. For this reason, we do not further discuss its value in this paper.

4. Discussion

The two quantities τ and A_V are in principle proportional. However the estimate of the dust optical depth τ requires to know the dust equilibrium temperature, requiring an additional step in the study of the dust/gas ratio, and additional assumptions that could bias the results. For instance, a single dust temperature is often assumed along the LOS. In addition, the temperature estimate depends on the assumption made on the emissivity spectral index β . In that sense, the use of extinction data is more straightforward. However, extinction data suffer from several defects, especially when producing the color excess map. Indeed, even if the X percentile method used to generate the map is a promising method, the resulting map can still be biased by missing extinction, inducing variations in the detection rate. Indeed, the detection rate, i.e., the fraction of the detected A_V to the true total A_V integrated along the LOS, could vary as a function of the Galactic coordinates and the distance to the clouds. In order to evaluate how much extinction we should miss in the adopted A_V map, we have carried out a test by applying the X percentile method to some artificial clouds set in the distribution of stars generated using the Besançon Model (Robin et al., 2003). First we prepared a spherical cloud having a Gaussian density distribution with a size of 6 pc (at FWHM) and with a total extinction along the LOS of $A_V = 10$ mag at the center of the cloud. We then located the cloud at realistic coordinates and distances of some nearby clouds in the simulated star distribution, e.g., at $(l,b)=(174.0^\circ, -13.5^\circ)$ and at $D=150$ pc for the Taurus cloud, and performed the X percentile method exactly in the same way as ? did using the 2MASS PSC. Results indicate that most of the individual clouds analyzed here are well detected with a detection rate larger than 90% (i.e., the model cloud with $A_V = 10$ mag is detected as $A_V > 9$ mag), except for Orion whose detection rate is $\approx 76\%$. General results show that nearby clouds ($D < 500$ pc), which represent most of the clouds at $|b| > 10^\circ$ in the A_V map, are well detected with a detection rate $> 80\%$ for all directions. The low $(A_V/N_H)^{\text{ref}}$ ratio derived in Orion could be the result of underestimating A_V in this region. Apart from this region, the $(A_V/N_H)^{\text{ref}}$ ratios in Table 1 appear equal or larger than the reference value given by Bohlin et al. (1978), confirming that the X percentile method does not breed substantial missing extinction.

The determination of the X_{CO} conversion factor is different from one analysis to another. Our average value of 1.67×10^{20} H₂ cm⁻²/(K km s⁻¹) is close to the Galactic average (Strong & Mattox, 1996) and the value derived by Dame et al. (2001) for $|b| > 5^\circ$. A decrease in X_{CO} is observed from the inner to the outer high latitude sky. Most of the clouds observed in the extinction map at $|b| > 10^\circ$ are nearby local clouds, at a distance of about 200-500 pc, so we do not interpret the variations as a result of the metallicity gradient (Rolleston et al., 2000). We attribute them to local variations. Arimoto et al. (1996), using CO data and virial masses, derived an average value near Sun of 2.8×10^{20} H₂ cm⁻²/(K km s⁻¹), with variations ranging from 2.09×10^{20} to 3.74×10^{20} H₂ cm⁻²/(K km s⁻¹) with increasing Galactocentric radius. Abdo, et al. (2010) evidenced a similar behavior, but with significant variations ranging from 0.87×10^{20} H₂ cm⁻²/(K km s⁻¹) in the Gould Belt to 1.9×10^{20} H₂ cm⁻²/(K km s⁻¹) in the Perseus arm. Finally, Planck collaboration (2011a) estimated an average value of 2.54×10^{20} H₂ cm⁻²/(K km s⁻¹) in the solar neighborhood. We also note that some of the studies included the dark component in their derivation of X_{CO} .

In their model to estimate the DG mass, Wolfire et al. (2010) predicted an HI-to-H₂ transition located at $A_V \approx 0.2$ mag, in

agreement with our findings. This result is however slightly lower than the value derived using FIR data ($A_V \approx 0.4$ mag) following Planck collaboration (2011a). However, in the latter case the HI-to- H_2 transition has been determined by χ^2 minimization whereas in our study it has been done by eye, which can induce large uncertainties.

Moreover, model predictions suggest a constant fraction of the molecular mass in the dark component of about 0.3 for an average extinction A_V around 8 mag. In cases of decreasing extinction, they found an increase in the dark mass fraction. In the framework of their model, this would indicate a more important fraction of the molecular gas located outside the CO region. This fraction (f_{DG}) is computed as:

$$f_{DG} = \frac{M_H^X}{M_H^X + M_H^{CO}}. \quad (7)$$

Values of f_{DG} for each region are provided in Table 1. Over the entire high latitude sky we derived $f_{DG} = 0.62$, with a larger value in the inner Galaxy ($f_{DG} = 0.71$) with respect to the outer Galaxy ($f_{DG} = 0.43$). For comparison, using the same definition of this quantity, Planck collaboration (2011a) obtained a value of $f_{DG} \approx 0.55$ for the solar neighborhood. The Taurus and Aquila-Ophiuchus regions evidence a DG fraction of 0.43 and 0.62, respectively. These values are in good agreement with the results obtained by Grenier et al. (2005) (see Table 1) in equivalent regions, with fractions of 0.3 and 0.6, for the Taurus and Aquila-Ophiuchus-Libra regions. These authors derived f_{DG} as low as 0.1 for Cepheus-Cassiopeia-Polaris and Orion, whereas Abdo, et al. (2010) deduced a value of 0.30 for Cepheus. We obtained f_{DG} equal to 0.15 and 0.40 in Cepheus-Polaris and Orion.

All these studies illustrate the existence of variations in the dark-gas mass fraction. In our study we exclude the Galactic plane, where the most massive and bright molecular clouds are located. At the $36'$ angular resolution most of the pixels considered in our analysis have extinction lower than 10 mag. In that case, f_{DG} values larger than 0.3 are expected following Wolfire et al. (2010), and this is indeed what is observed here.

Dust in the form of aggregates is likely to be more emissive with respect to isolated grains, but aggregation is not expected to substantially affect absorption properties in the visible (Kohler et al., 2011). The detection of significant departure from linearity between extinction data and gas column densities, especially in Orion or Aquila-Ophiuchus, that exhibit the largest excess in Figure 3, indicates that dust emissivity changes induced by grain aggregation is an unlikely explanation to the observed excess. As a consequence, grain coagulation can only be responsible of a small amount of the observed excess, and may explain some of the differences in the studies based on FIR data (Planck collaboration, 2011a) and visible extinction data (this work). Moreover, our results are in agreement with model prediction of Wolfire et al. (2010), favoring the hypothesis of pure H_2 gas (without CO molecules), surrounding the CO regions.

5. Summary

Using the recently revised all-sky extinction map, we have examined the correlation between extinction and gas column densities as derived from HI and CO observations. Our results can be summarized as follows:

- We have evidenced an excess of extinction at intermediate column densities, relative to a linear-fit between A_V and observable gas. This excess is observed over the whole high

latitude sky, with a predominant amount toward the inner regions ($|l| < 70^\circ$), and in Aquila-Ophiuchus in particular. This results confirm the recent detection of the DG in the Planck data and implies that the effect in the FIR is not due to changes in the dust optical properties due to dust aggregation.

- We have derived an average dust extinction to gas ratio $(A_V/N_H)^{ref} = 6.53 \times 10^{-22}$ mag cm^{-2} in the solar neighborhood, for an average $X_{CO} = 1.67 \times 10^{20}$ $H_2 cm^{-2}/(K km s^{-1})$. The inner/outer Galaxy exhibits a higher/lower $(A_V/N_H)^{ref}$ ratio ($8.72 \times 10^{-22}/5.46 \times 10^{-22}$ mag cm^{-2}), associated with a higher/lower X_{CO} factor ($2.28 \times 10^{20}/1.67 \times 10^{20}$ $H_2 cm^{-2}/(K km s^{-1})$). A significantly larger value, more than twice the value derived in the solar neighborhood is observed in the Aquila-Ophiuchus region. In contrast, the lowest X_{CO} value is found in Cepheus-Polaris.
- Results of our analysis are in agreement with theoretical predictions from modeling with the dark H_2 gas to explain the observed departure from linear-fits in the correlations.
- The DG mass derived is 19% of the atomic mass and 164% of that in the CO-traced gas in the solar neighborhood. It can reach up to 59% of the atomic gas in the Aquila-Ophiuchus region. Our DG mass estimates are slightly lower than that derived from FIR Planck data, but the difference is not significant.
- We have estimated the fraction of the molecular mass in the dark component (f_{DG}) and found an average value of 0.62 in the solar neighborhood, with variations going from 0.43 to 0.71 in the outer and inner Galaxy. We have derived $f_{DG}=0.15, 0.43, 0.40,$ and 0.62 in the Cepheus-Polaris, Taurus, Orion, and Aquila-Ophiuchus regions, respectively.
- The HI-to- H_2 and H_2 -to-CO transitions appear for $A_V \approx 0.2$ and $A_V \approx 1.5$ mag in the solar neighborhood, with variations from regions to regions.

Acknowledgements. D. P. was supported by the Centre National d'Etudes Spatiales (CNES). A part of this work was financially supported by Grant-in-Aid for Scientific Research (nos. 22700785 and 22340040) of Japan Society for the Promotion of Science (JSPS). The authors would like to thank T. M. Dame for making the unpublished CO data available to them to perform this work.

References

- Abdo, A. A., Ackermann, M., Ajello, M., et al. 2010, ApJ, 710, 133
 Arnal, E. M., Bajaja, E., Larrarte, J. J., et al. 2000, A&AS, 142, 35
 Arimoto, N., Sofue, Y., & Tsujimoto, T. 1996, PASJ, 48, 275
 Bajaja, E., Arnal, E. M., Larrarte, E., et al. 2005, A&A, 440, 767
 Bernard, J.-P., Reach, W., Paradis, D., et al. 2008, AJ, 136, 919
 Bohlin, R. C., Savage, B. D., & Drake, F. J. 1978, ApJ, 224, 132
 Cambrésy, L. 1999, A&A, 345, 965
 Cardelli, J. A., Clayton, G. C., & Mathis, J. S. 1989, ApJ, 345, 245
 Dame, T. M., Hartmann, D., & Thaddeus, P. 2001, ApJ, 547, 792
 Dame, T. M. 2011, arXiv:1101.1499
 Dame, T. M., et al., in preparation
 Dobashi, K., Bernard, J.-P., Hughes, A., et al. 2008, A&A, 484, 205
 Dobashi, K., Bernard, J.-P., Kawamura, A., et al. 2009, AJ, 137, 5099
 Dobashi, K., 2011, PASJ, 63, S1
 Dobashi, K., Marshall, D. J., Shimoikura, T., & Bernard, J.-P. 2012, PASJ, submitted
 Fukui, Y., Onishi, T., Abe, R., et al. 1999, PASJ, 51, 571
 Grenier, I. A., Casandjian, J. M., & Terrier, R. 2005, Science, 307, 1292
 Hartmann, D. & Burton, W. B. 1997, Atlas of Galactic Neutral Hydrogen, ed. Hartmann D. & Burton, W. B.
 Kohler, M., Stepnik, B., Jones, A. P., et al. 2011, A&A, in preparation
 Langer, W. D., Velusamy, T., Pineda, J. L., et al. 2010, A&A, 521, 17
 Lada, C. J., Lada, E. A., Clemens, D. P., & Bally, J. 1994, ApJ, 429, 694
 Leroy, A., Bolatto, A., Stanimirovic, S., et al. 2007, ApJ, 658, 1027
 Meyerdierts, H., & Heithausen, A. 1996, A&A, 313, 929
 Planck collaboration 2011a, Planck early results 17, A&A, 536, 17

Planck collaboration 2011b, Planck early results 24, A&A, 536, 24
 Reach, W. T., Koo, B., & Heiles, C 1994, ApJ, 429, 672
 Robin, A. C., Reylé, C., Derrière, S., & Picaud, S. 2003, A&A, 409, 523
 Rolleston, W. R. J., Smartt, S. J., Dufton, P. K., & Ryans, R. S. I. 2000, A&A, 363, 537
 Roman-Duval, J., Israel, F. P., Bolatto, A., et al. 2010, A&A, 518, 74
 Rowles, J., & Froebrich, D. 2009, MNRAS, 395, 1640
 Skrutskie, M. F., Cutri, R. M., Stiening, R., et al. 2006, AJ, 131, 1163
 Spitzer, L. 1978, Physical Processes in the Interstellar Medium (New-York: Wiley-Interscience)
 Strong, A. W., & Mattox, J. R., A&A, 308, 21
 Wolfire, M. G., Hollenbach, D., & McKee, C. F. 2010, ApJ, 716, 1191

Appendix A: WCS to HEALPix ancillary data transformation

The data used in this paper have been transformed from their native WCS (World Coordinate System) local projection into the HEALPix (Hierarchical Equal Area isoLatitude Pixelization) all-sky pixelization using the method described in this Appendix. This method was also used to produce HEALPix maps of a larger set of ancillary data. These have been used in particular, in the context of the analysis of the Planck data. The ancillary data produced this way can be accessed on <http://www.cesr.fr/~bernard/Ancillary/>. Note that the CO map used in this paper is not made available, since the corresponding data are not yet public.

The HEALPix format allows to store ancillary data on a single grid scheme on the sphere. This is an advantage since different data can then be compared on a pixel per pixel basis, without the need to project the data to a common grid. Ancillary data are available in the WCS convention and are usually stored as FITS files (Flexible Image Transport System). In the following, we call the ancillary data FITS maps. It is usually not practical to go back to the raw ancillary data and reprocess the maps into the HEALPix pixelization directly. It is therefore necessary to project the FITS format data into the HEALPix pixels. As the FITS and HEALPix pixels do not match in position, size and shape, this requires some kind of interpolation. This must be done with minimal loss of information and without altering the photometry of the original ancillary data. Here, we use a mosaicking method where we compute explicitly the surface of the pixel intersections, and use these values as weights to construct the HEALPix map.

The HEALPix pixels project onto a local FITS map as shown in Figure A.1. The calculations are performed for a HEALPix pixel size (given by the N_{side} HEALPix parameter) so that the corresponding HEALPix pixel size matches the Shannon criterion for the angular resolution of the data considered. This ensures that no spatial information is lost in the conversion and that the HEALPix and the FITS pixels have a similar size. For a given FITS projection (i.e. from the astrometry information contained in the FITS header), we first identify which HEALPix pixels intercept the sky area covered by the FITS map. For each of those HEALPix pixels, we identify the FITS pixels with a non-zero intersection. We then compute the surface fraction of the FITS pixels intersecting the HEALPix pixel S_{ih}^{if} , where if denotes the FITS pixel number and ih denotes the HEALPix pixel number.

The calculation is performed in the pixel space of the FITS map shown in Figure A.1. We first compute the sky coordinates of the four corners of the considered HEALPix pixel. We then transform these coordinates into 2D pixel numbers (i,j) of the FITS image using standard routines and the astrometry information contained in the FITS header of the considered

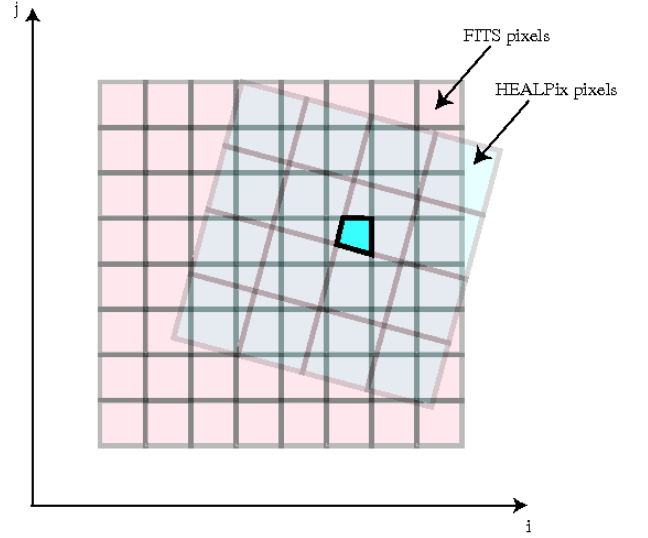


Fig. A.1. Geometry of the HEALPix and FITS pixels.

image. We then assume that the frontier of the HEALPix pixel is a straight line in the FITS image pixel frame. Although this is not exactly true, this is a very small approximation when the size of the HEALPix pixel is smaller or of the order of the FITS pixel size, which is always the case here. We then compute the surface of the corresponding intersection polygon, normalized to that of the HEALPix pixel surface S_{ih}^{if} . This calculation is performed using the *polyfillaa* routine (see <http://tir.astro.utoledo.edu/jdsmith/code/idl.php>) optimized for fast clipping of polygons against a pixel grid.

The intersection geometry informations (if and S_{ih}^{if}) are stored in a table containing one entry per HEALPix pixel with non-zero intersection with the considered FITS map. Calculations are carried and stored separately for each FITS map. Note that the above table can be easily inverted to a table with one entry per FITS pixel, giving the HEALPix pixel numbers intercepting it (ih) and the corresponding surface fraction S_{if}^{ih} , which in turn can be used for reverse calculations projecting HEALPix maps into local WCS projection.

The above intersection fractions are then used to compute HEALPix ancillary data value d_{ih} , given the FITS data d_{if} as

$$d_{ih} = \sum_{if} S_{if}^{ih} \times d_{if}. \quad (\text{A.1})$$

where the summation is carried over all FITS pixels intersecting HEALPix pixel ih .

When the data is composed of a collection of individual FITS maps, the calculation are performed for each map separately, while maintaining a map of the total weight, which allows to average values in sky regions where individual maps overlap. Note that virtually all WCS projection types can be used, including the sixcube projection used for the COBE and FIRAS data.